



Application of a Hygroscopicity Tandem Differential Mobility Analyzer for characterizing PM Emissions in exhaust plumes from an Aircraft Engine burning Conventional and Alternative fuels

5 Max B. Trueblood¹, Prem Lobo^{1,a}, Donald E. Hagen¹, Steven C. Achterberg¹, Wenyan Liu², Philip D. Whitefield¹

¹Center of Excellence for Aerospace Particulate Emissions Reduction Research, Missouri University of Science and Technology, Rolla, Missouri, USA 65409

²Center for Research in Energy and Environment, Missouri University of Science and Technology, Rolla, Missouri, USA 65409

10 ^aNow at: Measurement Science and Standards Research Centre, National Research Council Canada, Ottawa, Ontario, Canada K1A 0R6

Correspondence to: Max B. Trueblood (trueblud@mst.edu)

Abstract. In the last several decades, significant efforts have been directed toward better understanding the
15 Particulate Matter (PM) emissions from aircraft gas turbine engines. However, limited information is available on the hygroscopic properties of aircraft engine soot particles, in particular their soluble mass fraction (SMF). This parameter plays an important role in the water absorption, airborne lifetime, obscuring effect, and detrimental health effects of these particles. This study reports the description, detailed lab-based performance evaluation of a robust Hygroscopic-Tandem Differential Mobility Analyzer (H-TDMA) and subsequent field deployment to measure the SMF of aircraft engine soot particles in the
20 exhaust from CFM56-2C1 engines burning several fuels during the Alternative Aviation Fuel EXperiment (AAFEX) II campaign. The fuels used were a conventional JP-8, tallow-based hydro-processed esters and fatty acids (HEFA), Fischer-Tropsch, a blend of HEFA and JP-8, and Fischer-Tropsch doped with Tetrahydrothiophene (an organosulfur compound). In all cases the SMF was observed to increase with fuel sulfur content and engine power condition. SMF decreased with increasing particle size. The highest SMFs (~80%) were found in the smallest particles, typically those with diameters of 10
25 nm.

1 Introduction

30 The increase in aviation related activities has led to concern about the emissions from aircraft operations and their impact on local air quality (Unal et al., 2005; Woody et al., 2011), global climate (Lee et al., 2009; Brasseur et al., 2016) and health (Levy et al., 2012; Brunelle-Yeung et al., 2014). The primary products of conventional jet fuel combustion are NO_x, UHC, CO, SO_x,



CO₂, H₂O, and soot aerosol or soot particulate matter (PM). As the aircraft engine exhaust plume expands, mixes with ambient air, and cools, volatile compounds present in the gas phase at the engine exit plane undergo gas-to-particle conversion, and begin to condense on existing soot particles and form new particles (Onasch et al., 2009; Lobo et al., 2012; Timko et al., 2013). The black carbon component of the soot aerosol is referred to as non-volatile particulate matter (nvPM), while the volatile component consists of sulfates, nitrates, and organic compounds (Onasch et al., 2009). The composition of the volatile PM in the expanding aircraft engine exhaust plume varies greatly and depends on a number of factors such as fuel composition, ambient meteorological conditions, and plume age (Lobo et al., 2007; Lobo et al., 2012; Timko et al., 2013; Lobo et al., 2015a).

The aviation sector has been focussed on developing and implementing alternative fuels for use by airlines to diversify fuel supplies and mitigate aircraft engine emissions. The American Society for Testing and Materials (ASTM) and other fuels specification bodies have established a standard specification for the manufacture of aviation turbine fuel consisting of conventional and synthetic blending components under ASTM D7566 (ASTM, 2016). The pure alternative fuels have low to negligible amounts of aromatic, naphthalenes, and sulfur content when compared to conventional jet fuel. Studies have shown that non-volatile particulate matter (nvPM) and sulfur oxides emissions are dramatically reduced during alternative fuel combustion in aircraft engines (Timko et al., 2010; Lobo et al., 2011; Beyersdorf et al., 2014; Moore et al., 2015; Lobo et al., 2015b; Lobo et al., 2016). The nvPM at the engine exit plane is hydrophobic, but as the nvPM evolves in the dispersing plume its aging results in enhanced hydrophilicity (Weingartner et al., 1997; Zhang et al., 2008).

Investigation of atmospheric pollution, and in particular atmospheric visibility, has shown that aerosol optical properties are affected by size, composition, and hygroscopic growth of particles (Tang et al., 1981; Horvath, 1995; Kim et al., 2006; Meier et al., 2009). In urban environments, emissions from vehicles including soot, sulfates, and nitrates have been found to be the main contributors to visibility degradation (Ferron et al., 2005; Kim et al., 2006).

Hygroscopic-Tandem Differential Mobility Analysis (H-TDMA) systems have been widely used to measure the hygroscopic growth properties of PM in the sub-saturated regime in different environments (Massling et al., 2007; Swietlicki et al., 2008; Park et al., 2009b; Wu et al., 2013). H-TDMA measurements of soot aerosol from jet engine combustors (Gysel et al., 2003; Popovicheva et al., 2008) have also been performed. However, the application of an H-TDMA system to measure the hygroscopic properties of PM emissions measured in evolving aircraft engine exhaust plumes from the combustion of different fuels has not been previously performed.

For field measurements, where the ambient temperature and humidity cannot be controlled very closely, the H-TDMA system must be fairly rugged, stable, and versatile. The Missouri University of Science and Technology (MST) has developed a H-TDMA system to quantify the hygroscopic growth factor and soluble mass fraction of soot aerosol emitted from aircraft engines. The H-TDMA system was automated to operate such that it could determine SMF for an aerosol in approximately 45s. This is critical when conducting aircraft engine emission tests which can be quite expensive, and where the expanding exhaust plumes are subject to perturbations in wind speed and wind direction. This paper reports the results of lab-based experiments to evaluate the performance of the MST H-TDMA system, and in-field measurements of PM emissions in exhaust



plumes from the combustion of conventional and alternative fuels in a CFM56-2C1 engine during the Alternative Aviation Fuels EXperiment (AAFEX) II field campaign.

2 Experimental Method

- 5 The MST H-TDMA system consists of two differential mobility analyzers (DMAs), a humidifier (HUM) and a condensation particle counter (CPC). Fig 1 presents the schematic of the MST H-TDMA system. The polydisperse aerosol is first pre-conditioned by passing it through an ice bath (IB-0) to dry the sample and return it to room temperature with a saturation ratio of ~ 0.15 . The aerosol is then brought to charge equilibrium by passing it through a bipolar charger (BC), which contains 500 μCi of Polonium-210 prior to entering the first DMA (DMA1). The DMAs used in the H-TDMA system were custom designed and have been used in previous studies to classify aerosols based on electrical mobility (Schmid, 2000). The DMAs were of cylindrical geometry and had the following dimensions: effective inner length of 72.77 cm, and a sample flow annulus with an inner diameter of 5.07 cm and an outer diameter of 8.88 cm. The aerosol flow rate Q_p was set to 3 Lm^{-1} and the sheath flow rate, Q_s , was adjusted to 15 Lm^{-1} using mass flow meters (GFM 371, Aalborg Instruments) which are calibrated periodically. In DMA1, the poly-dispersed aerosol was classified, and monodisperse particles with a “dry” size, X_d , were selected. The excess flow in the DMA was recirculated as Q_{s1} , after passing through a second ice bath (IB-1) and a HEPA filter further ensuring that the sample remains dry and has not prematurely deliquesced to a solution droplet. DMA1 is set at a fixed voltage permitting the selection of a monodisperse aerosol. The monodisperse sample flow (Q_{m1}) out of DMA1 now enters the humidifier (HUM) section of the H-TDMA system, where it is now referred to as the polydisperse flow Q_{p2} . The HUM brings the aerosol sample to a controlled, precisely known humidity or saturation ratio (SR), typically 92 - 99%, which causes the particles to deliquesce to a new equilibrium “wet” diameter (X_w). Valves V2 and V3 can direct the aerosol flow Q_{p2} to either pass through the HUM (wet mode) or to bypass it (dry mode). Valves V4 and V5 achieve the same function for the sheath air flow Q_{s2} . The third ice bath (IB-2) in the Q_{s2} loop removes the water vapor from Q_{s2} and minimizes any unwanted vapors derived from the combustion process. The second DMA (DMA2) in conjunction with a CPC (TSI 3022) measures X_w . The MST H-TDMA system is designed to provide only one SR condition, and to hold that value regardless of variations in ambient temperature and humidity or sampling duration. The water bath that encases HUM/DMA2 is thermostated by a refrigerated water re-circulator that controls the water temperature around the HUM/DMA2 to $16. \pm 0.1 \text{ }^\circ\text{C}$. The thermostating water passes alongside the Q_{p2} and Q_{s2} lines (not shown in figure). Thus the dew point achieved in the humidifier region will be well below room temperature. The thermostating water flow rate through the water bath surrounding HUM/DMA2 is approximately 5 Lm^{-1} .
- 30 The SR values in flows Q_{p2} and Q_{s2} are brought to near unity at $16 \text{ }^\circ\text{C}$ by passing the aerosol through stainless steel tubes lined with wet cloth. The flow Q_{p2} passes through 4 such tubes (11 mm ID x 762 mm L), thus having a total length of 3048 mm and a residence time of 5.8 s. The flow Q_{s2} passes through 8 similar tubes, thus having a total length of 6096 mm and a residence time of 2.3 s.



The flow Q_d in parallel with the CPC reduces the lag time (LT2) between when a voltage is imposed on DMA2 and when particles selected by that voltage reach the CPC. Theoretical studies have shown that the lengths of wet walled tubing should be sufficient to bring the Q_{p2} and Q_{s2} to very near $SR=1$ (Fitzgerald et al., 1980). Just before entering DMA2, the SR of Q_{s2} is measured by a dew point hygrometer (DPH) (Vaisala HMP247, Vaisala, Inc.).

5 During routine operation, to maximize the data acquisition frequency the system is controlled by a computer running a LabVIEW program (LV1). When the program is initiated, it(1) sets the desired voltage (HV1) in DMA1 causing it to deliver dry particles of diameter X_d , (2) waits long enough for this monodisperse aerosol to travel from DMA1 through the HUM and into DMA2, (3) sets the high voltage in DMA2 (HV2) to some fraction of that in DMA1 (typically $0.1 \times HV1$), and (4) causes HV2 to step through 104 increments such that the final value is a multiple of HV1 (typically $10 \times HV1$). During the stepwise
10 voltage increase of HV2, LV1 records (at 1 Hz) values of HV1, HV2, Q_{s1} , Q_{s2} , Q_d , P1, P2, DPH, CPC and elapsed time (dt). The operator provides the general region (in time) where the peak in CPC readings occurred and LV1 fits a quadratic function to the CPC time series. The quadratic function is differentiated and the value of dt at the maximum is obtained (dt_{max}). Based on calibrations performed previously, LV1 computes the lag time (LT2) between when a certain diameter of droplet is selected by DMA2 and when it arrives at the CPC. This lag time has been found to be a function of Q_{s2} and Q_{p2} . LV1 finds the value
15 of the high voltage on the central rod of DMA2 (HV2*) at that time ($dt^*=dt_{max}-LT2$). It then computes the wet diameter (X_w) of the solution droplet (using the operating equation of the DMA2), and finally computes the SMF. LVI was developed such that SMF could be determined on more than one X_d . The program changes the particle diameter produced by DMA1 before the end of the voltage sweep on DMA2. The new particle diameter selected does not arrive at DMA2 while the current HV2 voltage sweep is running, but does arrive immediately after that step has been completed. DMA2 can then immediately start
20 the sweep on this new wet diameter. Thus the time taken to flush the tubing and the HUM is not wasted. This reduces the time for performing HV2 sweeps on 12 different dry diameters to about 9 minutes.

Periodically experiments are performed wherein a challenge aerosol of a pure inorganic salt ($(NH_4)_2SO_4$, NaCl, KI or KCl) (SMF=1) is used to validate/update the calibration of the dew point hygrometer DPH (as described in Suda et al., 2013). During an automated stepwise increase of HV2, the diameters X_d and X_w are precisely determined. The calculated saturation
25 ratio (SR-calc) is obtained from knowledge of the dry diameter X_d , the wet diameter X_w and the fact that the chemical is pure (SMF=1). The SR-calc is computed and compared to the value reported by the dew point hygrometer, SR_{DPH} . A calibration for the DPH { SR_{DPH} , SR-calc} is obtained. Typically, a value of 0.85 to 0.99 is obtained for SR-calc.

In the MST system, the SR is measured in the growth region by performing experiments (as recommended by Johnson et al., 2008). The SR is a function of not only the water vapor-air mixing ratio, but also a function of gas temperature. Even though
30 the mixing ratio will not change as Q_{s2} travels from the region of the DPH to the middle of the DMA2, the temperature may, resulting in a potential change in SR. Thus it is better to self-calibrate the H-TDMA using this method. Furthermore, it is generally known that reliable measurements of SR from commercial instruments become very hard to obtain the closer one gets to $SR=1$.



All H-TDMA systems described in the literature are designed to provide very precise values for the growth factor ($GF = X_w/X_d$). Furthermore almost all of these systems have the ability to vary the SR, thus requiring separate thermostating for the HUM and for DMA2 (Suda et al., 2013; Woods et al., 2013; Shi et al., 2012; Fors et al., 2010; Park et al., 2009a; Massling et al., 2011; Hu et al., 2010; Biskos et al., 2006; Lopez-Yglesias et al., 2014). Others (Johnson et al., 2008; Cubison et al., 2005) utilize controlled mixing of humid and dry air to achieve the desired humidity. Some systems include water baths (Hennig et al., 2005; Weingartner et al., 2002); temperature controlled cabinets (Cocker et al., 2001) and passive, insulated regions (Virkkula et al., 1999; Johnson et al., 2008).

Although these designs offer very good precision and the ability to vary the SR, they may not be well suited for field measurements, since most of them involve two separate volumes that must have their temperatures maintained very precisely. It is the temperature difference between these two volumes that is the critically important parameter. The MST H-TDMA system was designed to be less susceptible to ambient temperature fluctuations. This was achieved by encasing both the HUM and DMA2 in the same thermostated container (volume ~ 14 L). Other systems have also immersed DMA2 and the HUM in a water bath (Cubison et al., 2005; Hennig et al., 2005; Weingartner et al., 2002) to minimise the temperature gradients. In the MST H-TDMA system, temperature drifts are not critical, since the temperature difference between the HUM and the DMA2 (and the exposure time of the Q_{p2} and Q_{s2} in the HUM) is what determines the SR and that remains constant (zero temperature difference).

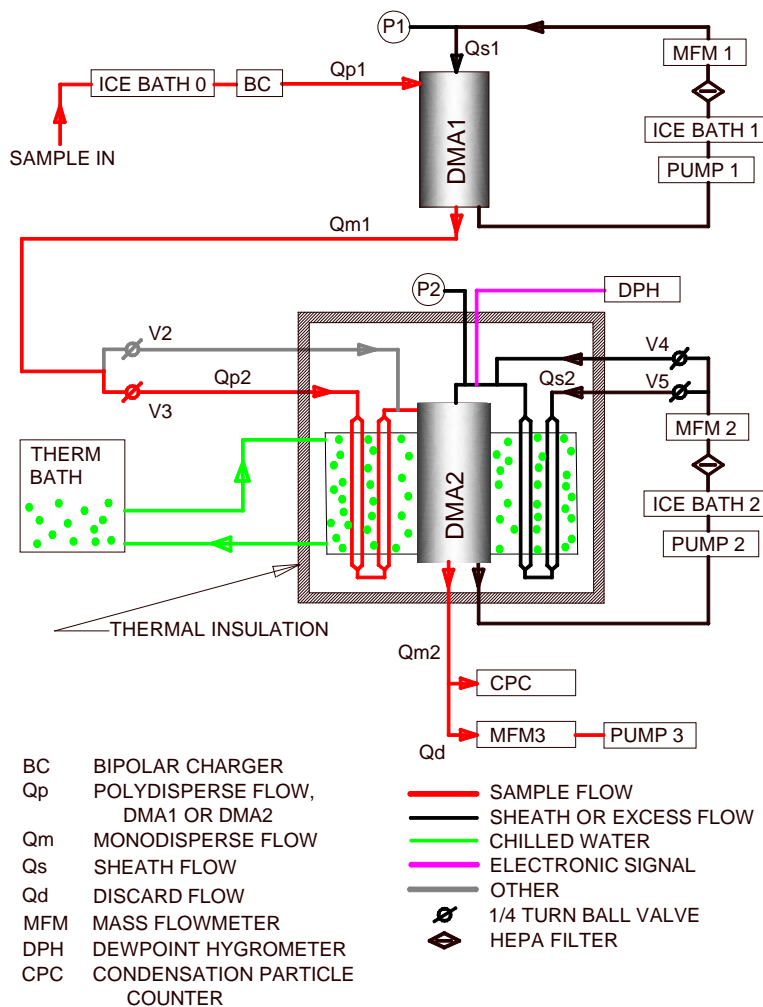


Fig. 1. The H-TDMA is comprised of two DMAs (DMA1 and DMA2) with a humidifier (HUM) between them. Valves can be turned to direct the gas flows to pass through or bypass the HUM. Thermostated water is pumped through the reservoir that surrounds both the HUM and DMA2.

5

Suda et al., 2013 discuss the problem of DMA offset, whereby the diameter as measured by DMA1 may be slightly different from the diameter as measured by DMA2, even if they both sample the same aerosol simultaneously. This situation is avoided in the MST system by performing a self-calibration. To accomplish this, an inorganic challenge aerosol (e.g. $(\text{NH}_4)_2\text{SO}_4$) is delivered to DMA1 and LV1 directs DMA1 to deliver a given diameter X_d particle. The HUM is bypassed and LV1 initiates voltage sweep on DMA2, which yields a diameter X_{wswp} . This is repeated for a series of X_d values ranging from 10 to 160 nm, establishing a calibration curve between X_d and X_{wswp} with X_d taken as the true diameter. Within LV1, this calibration is

10



then later utilized to synchronize the two DMAs. Since DMA1 is static during a voltage sweep and its X_d involves no error from uncertainties in the lag time (LT2), DMA1 is chosen as the reference.

3 Soluble mass fraction

5 In order to calculate the mass fraction of the aerosol that is soluble in water (Soluble Mass Fraction, SMF), information about the soluble and insoluble components is required. A dry hybrid particle with diameter X_d that is a mixture of a known type of soluble material on an insoluble core of diameter X_u will deliquesce to a new equilibrium wet diameter, X_w , when it is exposed to water vapor of sufficiently high SR. The dry diameter X_d can be experimentally determined by using DMA1. The density of the insoluble and soluble portions, ρ_u and ρ_s , respectively, are assumed to be known. It is assumed that the insoluble core of
 10 the aircraft engine particles is made up of black carbon. Recent studies have shown that a density of 1.0 g cm^{-3} is a reasonable approximation of the aircraft engine type used in this study (Durdina et al., 2014).

The insoluble core diameter, X_u can be computed from Köhler theory (Pruppacher et al., 1978) using the equations:

$$15 \quad SR = 1 + \frac{2A}{X_w} - \frac{8B}{(X_w^3 - X_u^3)} \quad (1)$$

$$A = \frac{(2 M_w \sigma_{w/a})}{R T \rho_w} \sim \frac{(3.3 \cdot 10^{-5})}{T} \quad (2)$$

$$20 \quad B = \frac{4.3 \nu m_s \Phi_s}{M_s} \quad (3)$$

where, M_w is the molecular weight of water, $\sigma_{w/a}$ is the surface tension of water against air, R is the universal gas law constant, T is the absolute temperature, ρ_w is the density of water, M_s is the molecular weight of the solute, ν is the number of ions into which the soluble salt disassociates, and Φ_s is the osmotic coefficient of the solution droplet.

25 The mass of the water soluble portion of the particle is given by:

$$m_s = (\pi/6) \rho_s (X_d^3 - X_u^3) \quad (4)$$

The insoluble portion will have a mass

$$30 \quad m_u = \left(\frac{\pi}{6}\right) (\rho_u X_u^3) \quad (5)$$

The SMF of this hybrid particle is defined as



$$SMF = \frac{m_s}{(m_s + m_u)} \quad (6)$$

If the dry particle does not contain an insoluble part, then the X_u in the denominator of Eq. (1) disappears ($X_u = 0$), leaving the more commonly used Köhler equation. Several researchers (Hamer et al., 1972; Robinson et al., 1959; Staples, 1981) have tabulated osmotic coefficients for selected solute materials as a function of the molality. We find that Φ_s can be related to the square root of the molality (ψ) by a 6th order polynomial function with considerable accuracy. Hence Φ_s is diameter dependent, and must be taken into account. The molality (ψ) (number of moles of the solute / mass of solvent in kg) is given by:

$$\psi = \frac{n(\text{solute})}{\text{mass of solvent (kg)}} = \frac{1000 \left(\frac{\pi}{6}\right) \rho_s (X_d^3 - X_u^3) M_s^{-1}}{\left(\frac{\pi}{6}\right) \rho_w (X_w^3 - X_d^3)} = \frac{1000 \rho_s (X_d^3 - X_u^3)}{\rho_w M_s (X_w^3 - X_d^3)} \quad (7)$$

where n is the number of moles of the solute. Solving Eq. (1) for m_s and equating to Eq. (2) gives

$$m_s = \left[\frac{(X_w^3 - X_u^3) M_s}{34.4 v \Phi_s (X_d, X_u, X_w)} \right] \left(1 + \frac{2A}{X_w} - SR \right) = \left(\frac{\pi}{6}\right) \rho_s (X_d^3 - X_u^3) \quad (8)$$

Solving for X_u

$$X_u = \left\{ 8 \frac{\left[\left(\frac{\pi}{6}\right) \rho_s \Phi_s X_d^3 - \left(\frac{X_w^3 M_s}{34.4 v}\right) \left(1 + \frac{2A}{X_w} - SR\right) \right]}{\left[\left(\frac{4\pi}{3}\right) \rho_s \Phi_s - \left(\frac{M_s}{4.3 v}\right) \left(1 + \frac{2A}{X_w} - SR\right) \right]} \right\}^{1/3} \quad (9)$$

It should be noted that Φ_s has an X_u dependency. Therefore Eq. (9) is solved iteratively using a non-linear equation solver with an initial guess of $\Phi_s = 1$ (very dilute solutions).

25 4 MST H-TDMA performance evaluation

4.1 Performance evaluation using pure inorganic salts

The performance of the H-TDMA system was evaluated by measuring the growth factor ($GF = X_w/X_d$) of pure inorganic salts for which GF can be calculated theoretically. The values of GF vs. X_d were measured and plotted for NaCl, $(NH_4)_2SO_4$, KI and KCl in Fig. 2. To obtain the theoretical GF, the SR-calc for the largest two or three dry particle diameters was computed and an average was obtained. This SR-calc value was then used to compute the theoretical GF for the smaller particle diameters. There is excellent agreement between the measured growth factor and the value predicted from theory. It should also be noted that the osmotic coefficient Φ_s is quite different from unity in several of the cases.



The dry diameter estimate (X_d) requires a knowledge of the average particle diameter actually exiting DMA1. A weighted average (neglecting doubly charged particles) is given by:

$$X_d = X_{avg} = \sum_{k=1}^N (SNN_k * X_k * F_k * TF_k * d\log X_k) / (\sum_{k=1}^N SNN_k * F_k * TF_k * d\log X_k) \quad (10)$$

5

where SNN_k is the differential size distribution entering the H-TDMA system (here measured by a DMS500, Cambustion, Ltd), X_k is the particle diameter, F_k is the fraction of particles of diameter X_k that carry one elementary charge (Hagen et al., 1983), TF_k is the transfer function of DMA1, and $d\log X_k$ is the differential in $\log X$ between adjacent data points in SNN_k .

The use of Eq. (10) rather than the DMA1 set point value for the average particle diameter provided a more accurate X_d value for these pure chemicals. The DMS500 reported the peak in SNN_k was at approximately 27 nm, for the nebulizer and the solutions of pure solute chemicals used. Since SNN_k and F_k were both monotonically increasing over the range where TF_k was nonzero, the X_{avg} was greater than what the DMA1 was tuned to. For example, when DMA1 was set to extract particles with $X_d = 12.76$ nm, the value of X_{avg} from Eq. (10) was found to be 13.49 nm which resulted in a change to the GF from 2.33 to 2.22 (a 5% correction). This correction was taken into account for particle diameters less than 20 nm. For particles diameters larger than 20nm, the correction is insignificant. This correction can be utilized for any diameter X_d as long as the SNN_k , the F_k , and the TF_k are known.

Most data reported in the literature for H-TDMA systems are designed to scan the SR (called humidigrams) and report (1) the GF for a wide SR range ($0.20 < SR < 1$), and (2) the deliquescence relative humidity (DRH), i.e., the SR at which the dry particles very abruptly begin to take on liquid water and grow to a much larger solution droplets. The MST H-TDMA system was not designed to perform humidigrams. By inspection of other humidigrams in the literature and with knowledge of the SR that was recorded in the MST H-TDMA, the GF can be estimated at this SR. Table 1 lists the GF at specific X_d values for various inorganic salts reported in the literature. There is good agreement between these values and those from this present study, as shown in Figs 2 (a)-(d).

25 **Table 1: Growth Factor at specific X_d values for various inorganic salts reported in the literature**

Study	Inorganic Salt	X_d (nm)	GF
Shi et al., 2012	NaCl	100	2.6
Mikhailov et al., 2004	$(NH_4)_2SO_4$	99	1.9
Johnson et al., 2008	$(NH_4)_2SO_4$	97	2.13
Park et al., 2009	KCl	20	2.05
Park et al., 2009	KCl	30	2.25

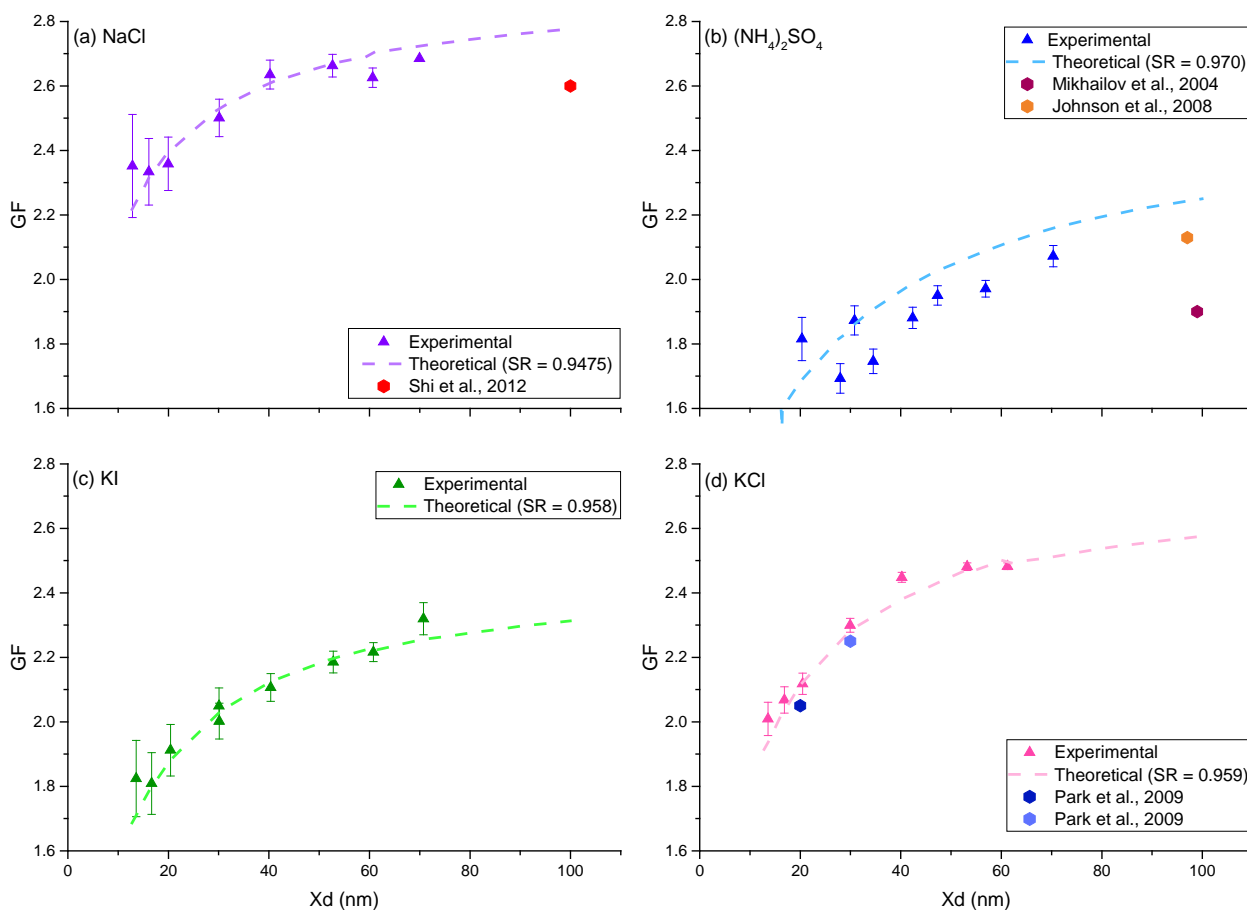


Fig. 2. Growth factor (GF) as a function of dry particle diameter (X_d) for Sodium Chloride (NaCl) (a), Ammonium Sulfate ($(\text{NH}_4)_2\text{SO}_4$) (b), Potassium Iodide (KI) (c), and Potassium Chloride (KCl) (d). Although not shown, the osmotic coefficient Φ_s varied from 1.1 at 10 nm to 1.0 at 65 nm for NaCl, 0.7 at 10 nm to 0.6 at 65 nm for $(\text{NH}_4)_2\text{SO}_4$, 1.05 at 10 nm to 0.95 at 65 nm for KI, and 1.0 at 10 nm to 0.9 at 65 nm for KCl.

4.2 Residence time

Since the deliquescence technique is an equilibrium based methodology, the closeness to equilibrium must be validated, especially for the larger droplets (which grow more slowly). For such a test, the apparatus was configured to select a dry diameter ($X_d = 17$ nm, 30 nm, or 51 nm) of $(\text{NH}_4)_2\text{SO}_4$ aerosol. The wet diameter (X_w) was measured, allowing calculation of GF and SR. This was repeated for a series of Q_{p2} values, which varied the residence time. The results are shown in Fig. 3.

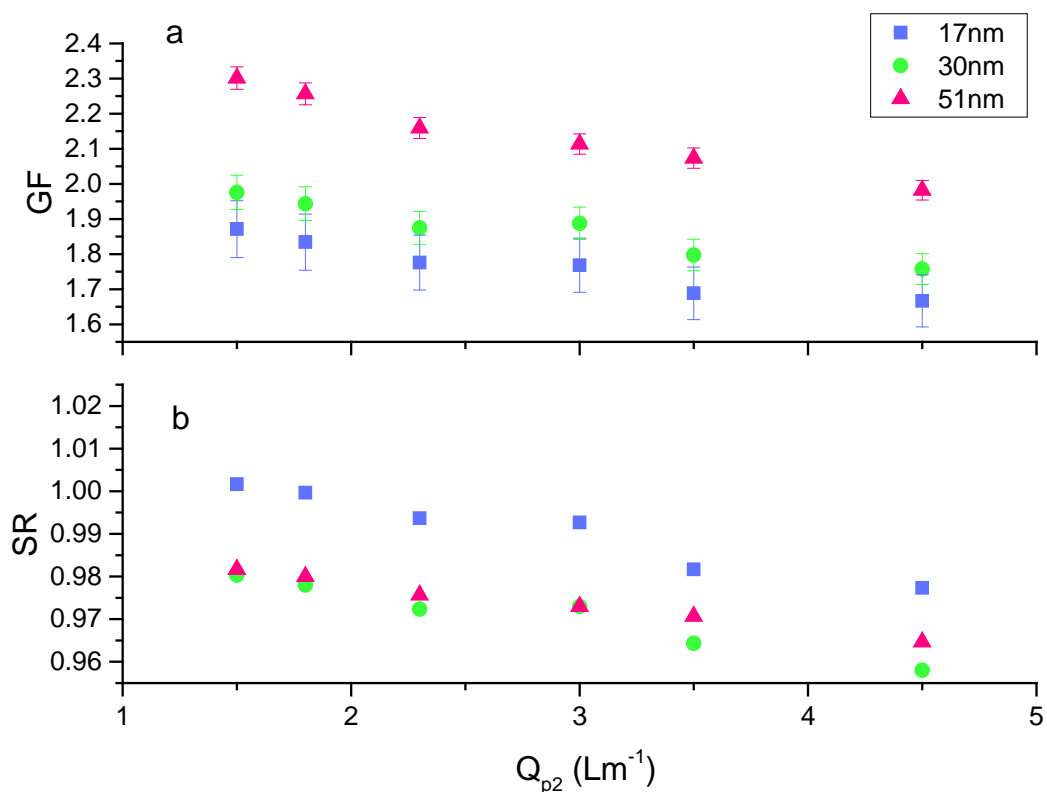


Fig. 3. Growth Factor (GF) (a), and Saturation Ratio (SR) (b) as a function of polydisperse flowrate Q_{p2} , with challenge $(\text{NH}_4)_2\text{SO}_4$ aerosols of 17 nm, 30 nm and 51 nm.

5

From Fig. 3. (a) and (b), a small dependence of GF and SR on Q_{p2} is observed. Utilizing a small Q_{p2} would be best to achieve the highest SR. However, very small values of Q_{p2} cause the concentration delivered to the CPC to be very low. In field measurements where the sample is diluted with ambient air, the concentration is already quite low leading to signal to noise issues. Alternatively, at large values of Q_{p2} , the peak is too broad. To avoid both of these extremes the H-TDMA system was operated at $Q_{p2} = 3.0 \text{ Lm}^{-1}$.

The H-TDMA system, when deployed in the field, is primarily intended to study particles with small X_d values and small SMFs. These particles will probably not grow large enough to experience insufficient growth time problems. However, it is good practice to periodically check the system and the sample aerosol by choosing a large X_d (say 30 nm or larger) to determine if changing the Q_{p2} results in a change to SR. If this is the case, then it is better to keep the Q_{p2} at a lower value (2.0 Lm^{-1}).

15



4.3 Stability over long operating times

For field applications, the H-TDMA system is required to maintain stable operation for long periods of time. The HUM tubes are wetted at the beginning of the day and need to be periodically rewetted to maintain a stable SR. The time after which the HUM tubes need to be rewetted was experimentally determined. Fig 4 displays the results of determining the SR by using particles of pure $(\text{NH}_4)_2\text{SO}_4$ ($X_u=0$ in Eq. (1)) and measuring the wet diameter X_w , given that the dry diameter set in DMA1 is held constant. Experiments were performed whereby the HUM tubes were wet thoroughly, and then automated scans were conducted for several hours with no further tube wetting. After the experimental measurements were performed, three elements of the set $\{X_d, X_w, \text{SR}, \text{SMF}\}$ were known, allowing calculation of the fourth, i.e., SR. Also shown is the measured SR of the Q_{sh2} as determined by the DPH. Fig 4 shows that the calculated and the measured SR remained quite constant for a period of over 225 minutes without having to rewet the tubes.

When required, tube rewetting is accomplished using a LabVIEW program which acts through a relay board (MN DB-24PRD, OMEGA Engineering, Inc.) to energize a peristaltic pump and sequentially open twelve pinch valves (PN 161P012, NResearch Inc.) for a short period (set by the operator), allowing each tube to be rewet in sequence. After rewetting, valves at the bottoms of the 12 stainless steel tubes are manually opened allowing excess water to drain. During normal operations in the field, the HUM tubes are rewetted every 150 minutes.

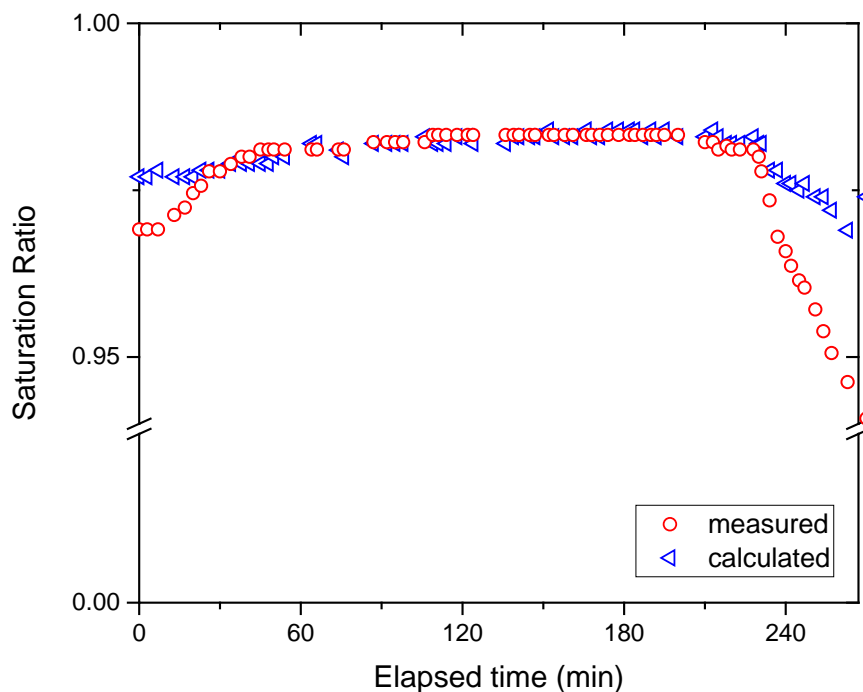


Fig. 4. SR as a function of elapsed time since last wetting for pure particles of $(\text{NH}_4)_2\text{SO}_4$. The uncertainty in the SR (calculated) is approximately 0.008.



4.4 Stability over varying ambient temperature conditions

Another performance verification test described here involves the behavior of the H-TDMA under varying ambient temperature conditions. The H-TDMA system was fed a challenge aerosol of pure $(\text{NH}_4)_2\text{SO}_4$. DMA1 was set to extract dry particles of 30 nm. An automated sweep with DMA2 was performed every 2 minutes, determining the X_w . The saturation ratio was computed using Eq. (1), with $X_u = 0$. At $t=20$ min (and 40 min), the environmental conditions surrounding the H-TDMA were abruptly changed by blowing cold air over the bottom of the HUM tubes (or not blowing cold air over the bottom of the HUM), which is not as well thermally insulated as the rest of the H-TDMA system (Fig. 1). This experiment was repeated four times on four different days. The SR remained quite constant over the duration of any one run as shown in Fig. 5. The average standard deviation in SR divided by the average SR for that trial over all four trials (120 measurements) was 0.0019, indicating that this system was insensitive to ambient temperature fluctuations.

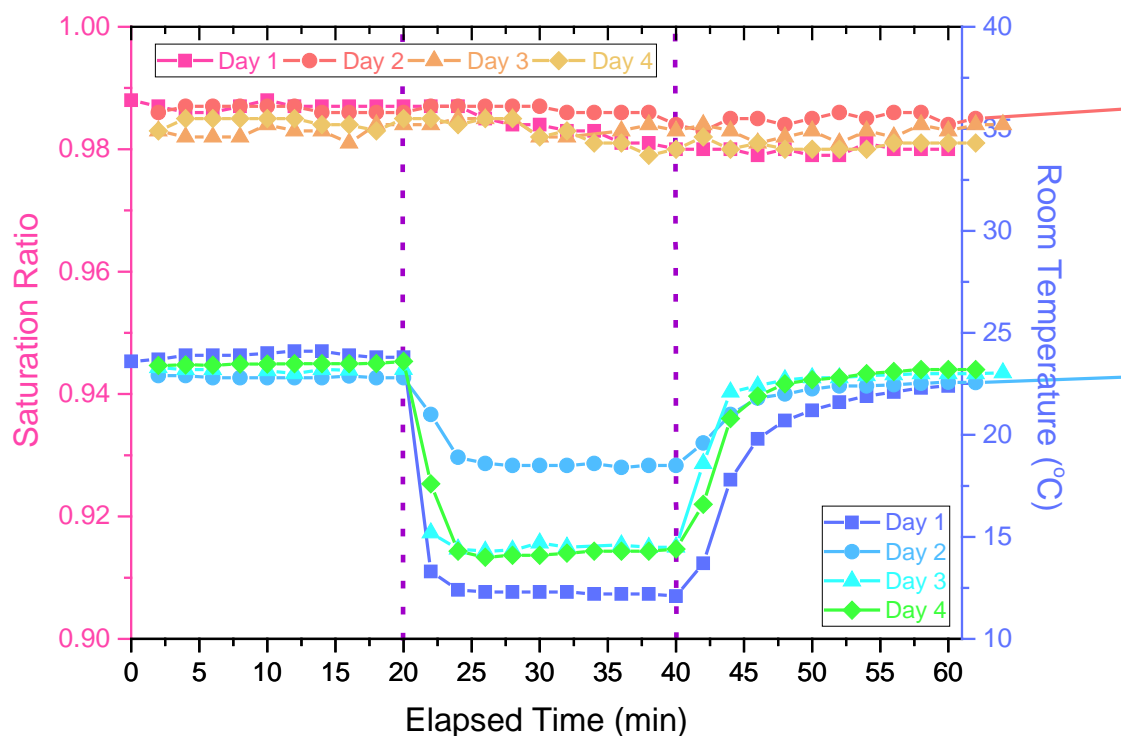


Fig. 5. Saturation Ratio and Room Temperature as a function of elapsed time



5 Field deployment during the AAFEX II campaign

The MST H-TDMA system was deployed as part of the Alternative Aviation Fuels EXperiment (AAFEX II) campaign conducted during 20 March - 2 April 2011 at the NASA Dryden Aircraft Operations Facility (DAOF), Palmdale, CA, USA. The NASA DC-8 aircraft equipped with CFM56-2C1 engines was utilized as the emissions source. The aircraft was parked in an open air run-up facility with no other aircraft or emission sources in the vicinity of the test site. Detailed descriptions of the test site and experimental set up have been previously reported (Timko et al., 2013; Moore et al., 2015). The main objective of the campaign was to investigate the gaseous and PM emissions characteristics of the CFM56-2C1 engine burning conventional and alternative fuels as a function of engine power conditions at several sampling locations in the exhaust plume. PM emissions data was acquired for a typical cycle which consisted of the following engine power conditions: 4%, 7%, 30%, 65%, 85% and 100% rated thrust. Two test cycles were run for each fuel – one stepping up from 4% to 100% rated thrust, and the other stepping down from 100% to 4% rated thrust. Five fuels were used during the campaign: (1) JP-8 (the military equivalent of conventional Jet A/JetA-1), (2) tallow-based hydro-processed esters and fatty acids (HEFA), (3) coal-derived Sasol Fischer-Tropsch (FT), (4) a blend of HEFA and JP-8, and (5) FT doped with Tetrahydrothiophene (THT) to boost the sulfur content of the fuel. A summary of selected fuel properties is provided in Table 2. Chemical and physical analysis of the HEFA and FT fuels has been reported elsewhere (Corporan et al., 2011).

Table 2. Selected fuel properties

Property	Method	JP-8	HEFA	FT	HEFA-JP-8 Blend	FT+THT
Density @ 15°C (kg/l)	ASTM D 4052	0.811	0.758	0.761	0.783	0.761
Viscosity @ -20°C (mm ² /s)	ASTM D 445	4.1	4.9	3.7	4.3	3.2
Distillation temperature (°C)	ASTM D 86					
10% recovered		168	175	164	166	164
End point		268	254	226	263	224
Flash Point (°C)	ASTM D 93	46	52	43	46	43
Net Heat of Combustion (MJ/kg)	ASTM D 4809	42.8	43.6	43.8	43.3	43.8
Aromatics (% vol)	ASTM D 1319	21.8	0.4	1.4	10.2	2.1
Naphthalenes (% vol)	ASTM D1840	1.3	0	0	0.65	0
Sulphur (ppm)	ASTM D 2622	188	6	4	276	1083
Hydrogen Content (% mass)	ASTM D 3343	13.5	15.3	15	14.4	15
Carbon content (% mass)	calculated	86.5	84.7	85	85.6	85
H/C ratio	calculated	1.86	2.15	2.10	2.00	2.10



The emissions from the CFM56-2C1 engine were measured at several distances (1 m, 30 m, 143 m) from the engine exit plane to study the PM characteristics as the exhaust plume cooled and mixed with ambient air. Only data acquired at the 143 m location will be presented and discussed here. A 2 inch ID aluminum tube positioned downwind from #3 engine on the starboard side of the aircraft was used to extract exhaust plume samples at this location. The exhaust was transported to a small trailer approximately 18 m away which housed the MST H-TDMA system to measure hygroscopic properties. Also housed in the trailer was a Cambustion DMS500 (Reavell et al., 2002; Hagen et al., 2009) which measured the real-time particle size distributions, and a LI-COR 840A NDIR detector that measured exhaust CO₂ concentration. The exhaust samples at 4% and 7% engine thrust conditions were impacted by the ambient conditions, specifically, wind speed and wind direction. However, the CO₂ measurements during the 7% thrust periods were approximately twice the background level, indicating that the exhaust plume was being sampled.

The sample to the DMS500 measured total PM size distributions, and nvPM size distributions were obtained by sending the sample through a thermal denuder. The thermal denuder consisted of a coil of stainless steel tubing (0.457cm ID) housed in a temperature controlled aluminium box heated to 300°C, followed by a cooling section. It is similar in design to that used by Saleh et al. (2011), and has been used in a previous study (Rye et al., 2012). Laboratory evaluations have demonstrated that H₂SO₄ droplets of diameter 10 – 100 nm are almost completely evaporated in the thermal denuder. Ambient meteorological conditions such as temperature, pressure, and relative humidity were also monitored and recorded throughout the campaign. The exhaust gas flow rate through the 2 inch ID x 18 m L tubing was well over 100 Lm⁻¹.

The total and nvPM number-based size distributions were converted to number-based emission index (EIn) distributions to account for varying amounts of dilution for each plume, and are presented for selected fuels at the 100% thrust condition shown in Fig. 6. The total PM size distributions are bi-modal with a strong nucleation mode (<20nm) and an accumulation mode. These observations are consistent with those reported for PM emissions measured downwind of several different aircraft engine types (Lobo et al., 2007; Lobo et al., 2012; Lobo et al., 2015a). The enhancement of the nucleation mode in measurements made downwind of the engine exit plane is due to gas-to-particle conversion in the exhaust plume driven by fuel composition, ambient conditions, and degree of mixing.

The sulfur in the fuel is oxidized to SO₂, which then undergoes rapid oxidation to SO₃ and subsequently to sulphuric acid (H₂SO₄) in the exhaust plume (Miake-Lye et al., 1998; Schumann et al., 2002). The H₂SO₄ either self nucleates to form pure H₂SO₄ droplets, or finds an existing soot particle to form a hybrid particle that subsequently has a significant water soluble component (Gysel, et al., 2003; Wyslouzil et al., 1994).

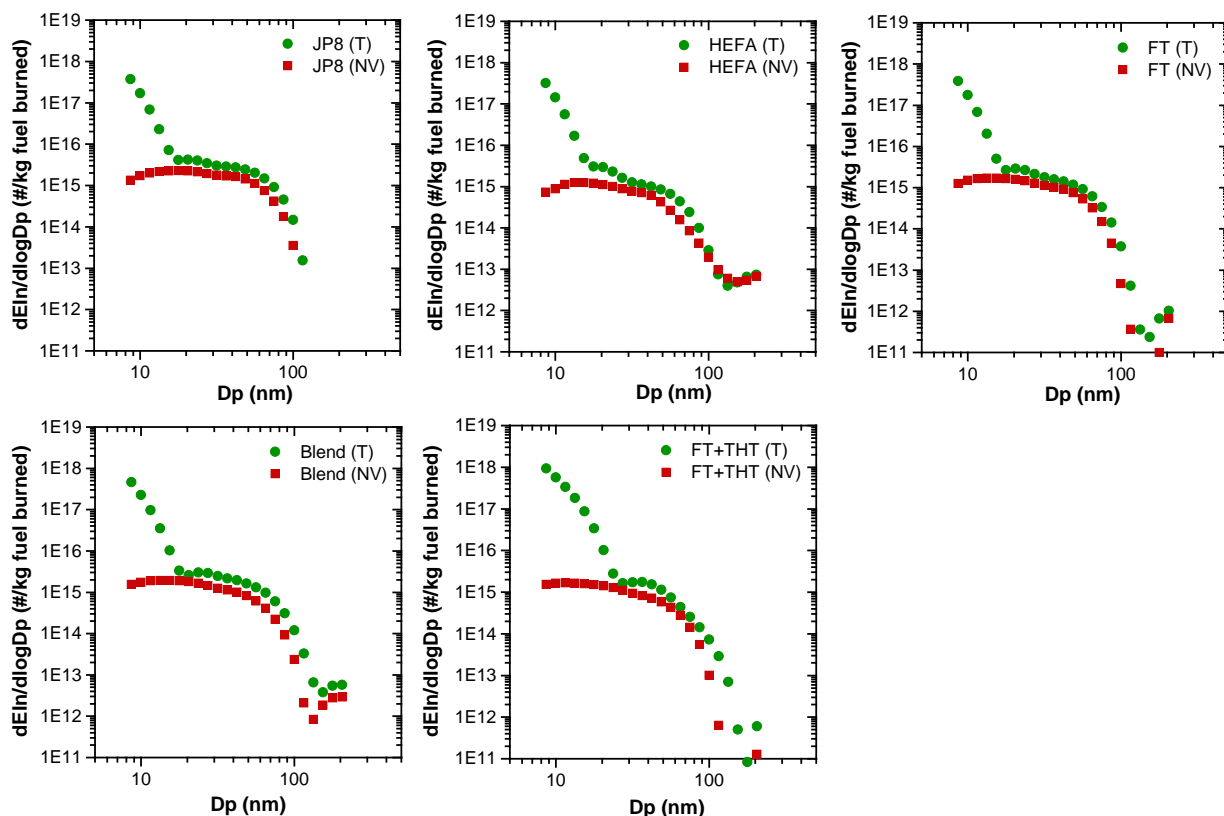


Fig. 6. Total (T) and non-volatile (NV) PM number-based emission index (EI_n) size distributions for the various fuels at the 100% thrust condition.

5 The data acquired with the MST H-TDMA system was used to calculate GF and SMF of these particles as a function of fuel type, engine thrust setting, ambient air temperature, and dry particle diameter. Fig. 7 shows the GF and SMF for the different fuels for the 7% thrust condition. For the FT and HEFA fuels, the GF and SMF are very close to zero, since they contain negligible amounts of sulfur. Gysel et al. (2007) state that sulfuric acid is expected to retain water at 5-10% RH, corresponding to a growth factor of ~ 1.15 , and took this into account when calculating the mixed particle growth factor in their data. This procedure was similarly followed for the current dataset. Thus the measured dry diameters were adjusted down by a factor of 0.869. Figs. 8 through 11 plot the GF and SMF vs. X_d for the other engine thrust levels and the different fuels. The H-TDMA was operated with a SR of 0.91.

10 Gysel et al. (2003) reported GF measurements for combustion particles from burning three different fuels with 50, 410, and 1270 μg of sulfur per g of fuel at old and modern cruise conditions. These results are included in the 85% engine thrust plots (Fig 10). This data is in good agreement with the current measurement data for very low sulfur (HEFA and FT) fuels, 15 regular JP8, and the sulfur enhanced FT respectively.

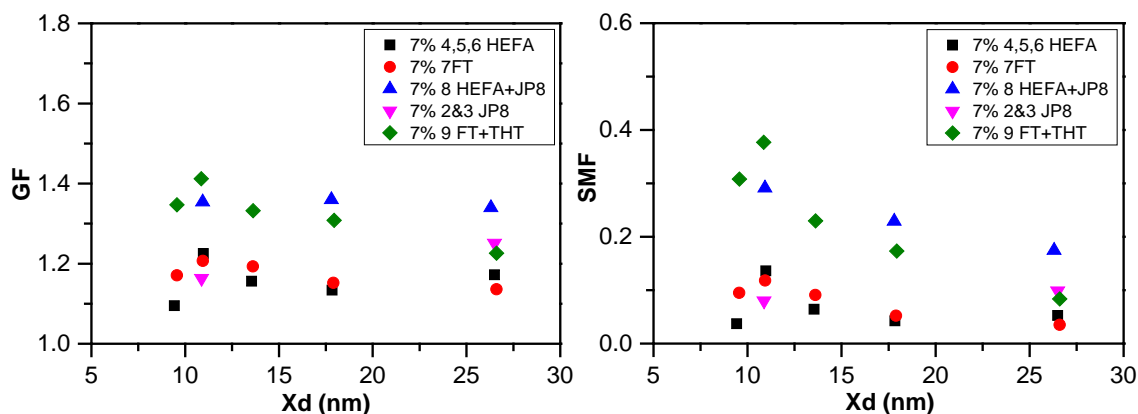
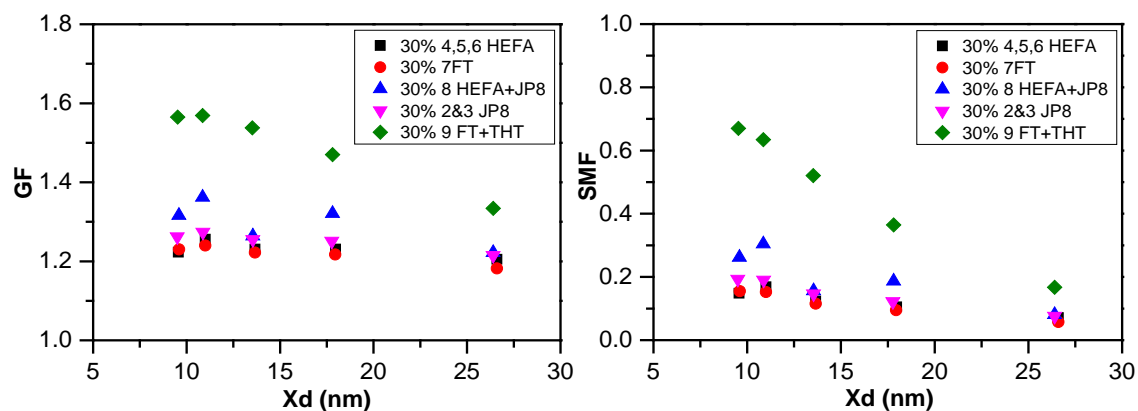


Fig. 7. GF and SMF vs. X_d for particles generated with an engine thrust level of 7% for different fuels.



5 Fig. 8. GF and SMF vs. X_d for particles generated with an engine thrust level of 30% for different fuels.

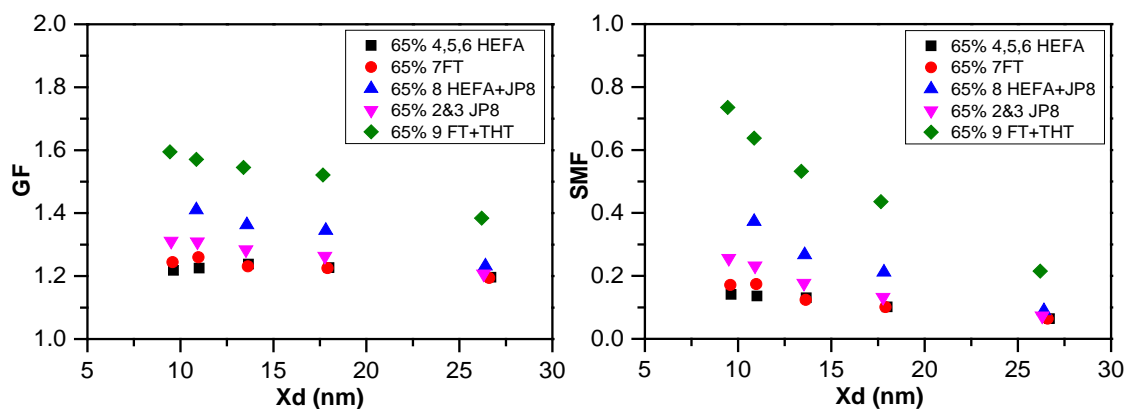


Fig. 9. GF and SMF vs. X_d for particles generated with an engine thrust level of 65% for different fuels.

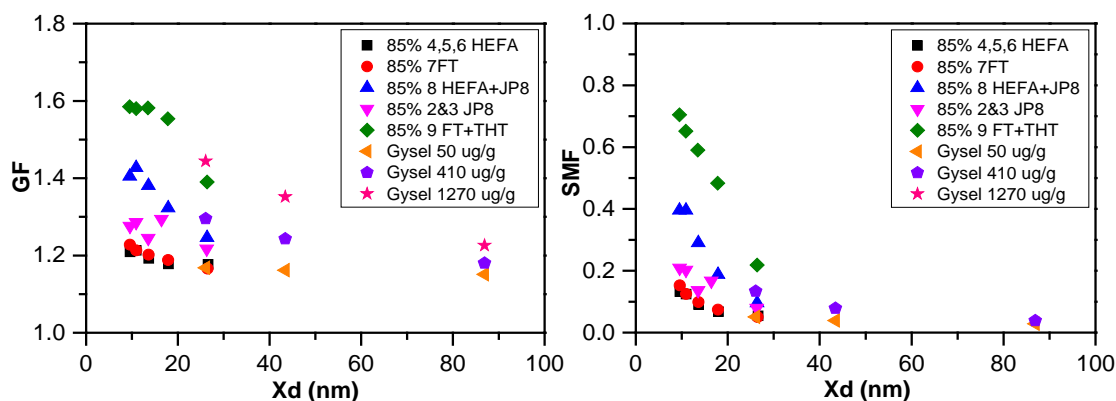
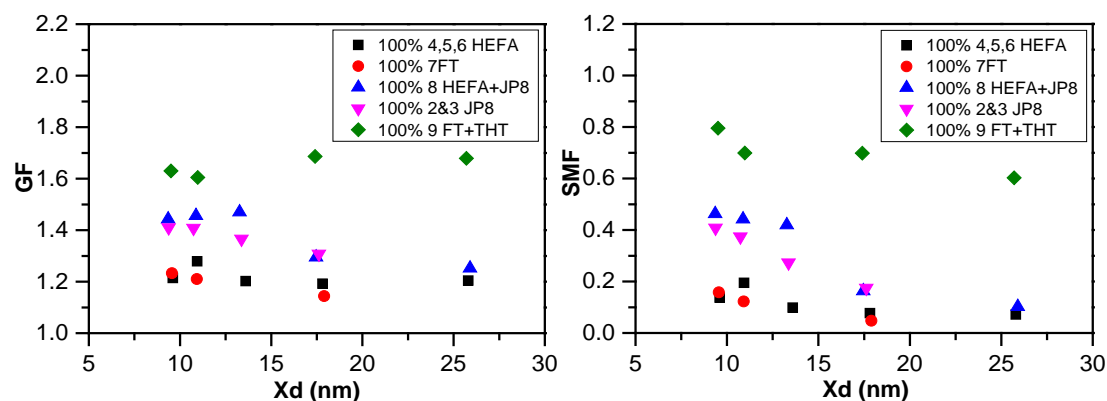


Fig. 10. GF and SMF vs. Xd for particles generated with an engine thrust level of 85% for different fuels.



5 Fig. 11. GF and SMF vs. Xd for particles generated with an engine thrust level of 100% for different fuels.

It was observed that as the FSC increased, so did the SMF. The SMF was observed to be dependent on particle diameter, with the highest SMF in particles around 10 nm. This mode, commonly termed the nucleation mode, is thought to be composed of particles or droplets formed by the homogeneous nucleation of low equilibrium vapor pressure species, such as H_2SO_4 . One might expect that these particles/droplets would be highly or completely soluble, and this is also borne out by the data. The SMF increases with increasing engine thrust level. The effect of engine thrust level on the GF is shown in Fig. 12. In these plots the GF is plotted versus the thrust level (TL). Notice that for runs 2 and 3 (JP8) and run 9 (FT plus THT) the GF is small then increases with TL to a more or less constant value, then increases again at high TL for all sizes.

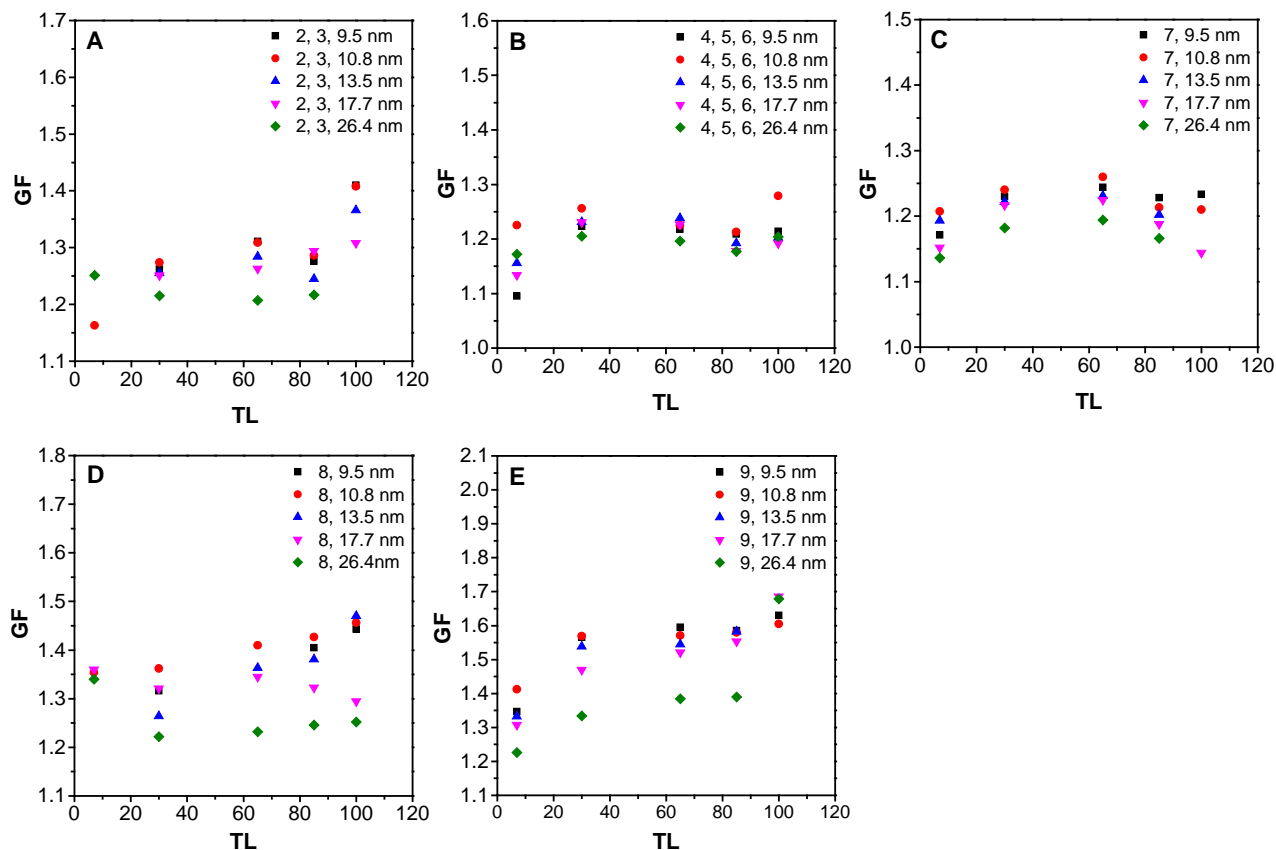


Fig. 12. GF vs. engine thrust level (TL) for runs (A) 2 and 3 (normal JP8), (B) 4, 5, and 6 (HEFA fuel), (C) 7 (FT fuel), (D) 8 (HEFA and JP8 Blend-1), and (E) 9 (FT plus THT).

5

6 Conclusions

A robust, mobile hygroscopicity tandem differential mobility analyzer has been developed. This H-TDMA was designed specifically for (1) field measurements involving mobile sources that are very costly to operate, (2) when exhaust sample plumes are available for only short periods of time, and (3) for varying ambient conditions. The GF exhibited by particles of four inorganic salts was studied and found to be in good agreement with theory and with the results of other investigators. The fixed SR provided by the apparatus (typically ~ 0.98) was found to be quite constant over long periods of time, even when the ambient temperature varied considerably, making this H-TDMA quite suitable for field experiments. This H-TDMA can do a SMF determination for one dry diameter in approximately 45 s. It can do as many as 12 dry diameters sequentially with one running of its LabVIEW control program in approximately 9 min. This H-TDMA was deployed during the field campaign Alternative Aviation Fuels EXperiment field campaign (AAFEX II). This H-TDMA provided significant findings on the GF



and SMF of particles in the exhaust. These findings are (1) SMF increased with fuel borne sulfur content, (2) SMF was observed to be diameter dependent and the highest SMF was found in the particles around 10 nm, and (3) the SMF increased with increasing engine thrust level.

5 Acknowledgements

This work was partly funded by the US Federal Aviation Administration (FAA) through the Partnership for AiR Transportation for Noise and Emissions Reduction (PARTNER) – an FAA-NASA-Transport Canada-US DoD-US EPA sponsored Center of Excellence Project 20 under Grant No. 09-C-NE-MST Amendment 003. Any opinions, findings, and conclusions or recommendations expressed in this paper are those of the authors and do not necessarily reflect the views of the FAA. We thank the entire AAFEX II project team for their support during the campaign. We also thank Veronica Villines Teat, Emitt Witt, Christian Hurst, Elizabeth Black, and Jonathon Sidwell for their assistance in gathering some of the data.

References

- ASTM International: Standard Specification for Aviation Turbine Fuel Containing Synthesized Hydrocarbons, ASTM D7566, West Conshohocken, PA, doi: 10.1520/D7566-16B, 2016.
- 15 Beyersdorf, A.J., Timko, M.T., Ziemba, L. D., Bulzan, D., Corporan, E., Herndon, S. C., Howard, R., Miake-Lye, R., Thornhill, K.L., Winstead, E., Wey, C., Yu, Z., and Anderson, B.E.: Reductions in aircraft particulate emissions due to the use of Fischer–Tropsch fuels, *Atmos. Chem. Phys.*, 14, 11–23, doi:10.5194/acp-14-11-2014, 2014.
- Biskos, G., Paulsen, D., Russell, L. M., Fouseck, P. R., and Martin, S. T.: Prompt deliquescence and efflorescence of aerosol nanoparticles, *Atmos. Chem. Phys.*, 6, 4633–4642, doi:10.5194/acp-6-4633-2006, 2006.
- 20 Brasseur, G. P., Gupta, M., Anderson, B. E., Balasubramanian, S., Barrett, S., Duda, D., Fleming, G., Forster, P. M., Fuglestedt, J., Gettelman, A., Halthore, R. N., Jacob, S. D., Jacobson, M. Z., Khodayari, A., Liou, K. N., Lund, M.T., Miake-Lye, R.C., Minnis, P., Olsen, S., Penner, J. E., Prinn, R., Schumann, U., Selkirk, H. B., Sokolov, A., Unger, N., Wolfe, P., Wong, H. W., Wuebbles, D. W., Yi, B., Yang, P., and Zhou, C.: Impact of aviation on climate: FAA’s Aviation Climate Change Research Initiative (ACCRI) Phase II., *Bull. Amer. Meteor. Soc.*, 97, 561–583, doi:10.1175/BAMS-D-13-00089.1, 2016.
- 25 Brunelle-Yeung, E., Masek, T., Rojo, J.J., Levy, J.I., Arunachalam, S., Miller, S.M., Barrett, S.R.H., Kuhn, S.R., and Waitz, I.A.: Assessing the impact of aviation environmental policies on public health, *Transport Policy*, 34, 21–28, doi: org/10.1016/j.tranpol.2014.02.015, 2014.
- Cocker, D. R., Flagan, R. C., and Seinfeld, J. H.: State-of-the-Art Chamber Facility for Studying Atmospheric Aerosol Chemistry, *Environ. Sci. Technol.*, 35, 2594–2601, doi: 10.1021/es0019169, 2001.
- 30 Corporan, E., Edwards, T., Shafer, L., DeWitt, M.J., Klingshirn, C., Zabarnick, S., West, Z., Striebich, R., Graham, J., and Klein, J.: Chemical, Thermal Stability, Seal Swell, and Emissions Studies of Alternative Jet Fuels, *Energy Fuels*, 25, 955–966, doi: 10.1021/ef101520v, 2011.



- Cubison, M. J., Coe, H., and Gysel, M.: A modified hygroscopic tandem DMA and a data retrieval method based on optimal estimation, *J. Aerosol Sci.*, 36, 846-865, doi:10.1016/j.jaerosci.2004.11.009, 2005.
- Durdina, L., Brem, B. T., Abegglen, M., Lobo, P., Rindlisbacher, T., Thomson, K. A., Smallwood, G. J., Hagen, D. E., Sierau, B., and Wang, J.: Determination of PM mass emissions from an aircraft turbine engine using particle effective density, *Environ.*, 99, 500-507, doi: 10.1016/j.atmosenv.2014.10.018, 2014.
- Ferron, G.A., Karg, E., Busch, B., and Heyder, J.: Ambient particles at an urban, semi-urban and rural site in Central Europe: hygroscopic properties, *Atmos. Environ.*, 39, 343-352, doi: 10.1016/j.atmosenv.2004.09.015, 2005.
- Fitzgerald, J., Rogers, J., and Hudson, C. F.: Review of isothermal haze chamber performance, *J. Rech. Atmos.*, 333-346, 1980.
- Fors, E. O., Rissler, J., Massling, A., Svenningsson, B., Andreae, M. O., Dusek, U., Frank, G. P., Hoffer, A., Bilde, M., Kiss, G., Janitsek, S., Henning, S., Facchini, M. C., Decesari, S., and Swietlicki, E.: Hygroscopic properties of Amazonian biomass burning and European background HULUS and investigation of their effects on surface tension with two models linking H-TDMA to CCNC data, *Atmos. Chem. Phys.*, 10, 5625-5639, doi:10.5194/acp-10-5625-2010, 2010.
- Gysel, M., Weingartner, E., and Baltensperger, U.: Hygroscopicity of aerosol particles at low temperatures. 2. Theoretical and experimental hygroscopic properties of laboratory generated aerosols, *Environ. Sci. Technol.*, 36, 63-68, doi:10.1021/es010055g, 2002.
- Gysel, M., Nyeki, S., Weingartner, E., Baltensperger, U., Giebl, H., Hitztenberger, R., Petzold, A., and Wilson, C. W.: Properties of jet engine combustion particles during the PartEmis experiment, Hygroscopicity at subsaturated conditions, *Geophys. Res. Lett.*, 30, 20-1 to 20-4, doi:10.1029/2003GL016896, 2003.
- Gysel, M., Nyeki, S., Paulsen, D., Weingartner, E., Baltensperger, U., Galambos, I., and Kiss, G.: Hygroscopic properties of water-soluble matter and humic-like organics in atmospheric fine aerosol, *Atmos. Chem. Phys.*, 4, 35-50, doi:10.5194/acp-4-35-2004, 2004.
- Hagen, D. E., and Alofs, D. J.: Linear inversion method to obtain aerosol size distributions from measurements with a differential mobility analyzer, *Aerosol Sci. Technol.*, 2, 465-475, 1983.
- Hagen, D.E., Lobo, P., Whitefield, P.D., Trueblood, M.B., Alofs, D.J., and Schmid, O.: Performance Evaluation of a Fast Mobility-Based Particle Spectrometer for Aircraft Exhaust, *J. Propul. Power*, 25, 628-634, doi: 10.2514/1.37654, 2009.
- Hamer, W.: Osmotic coefficients and mean activity coefficients of uni-univalent electrolytes in water at 25C, *J. Phys. Chem. Ref. Data*, 1, 1-54, 2009.
- Hennig, T., Massling, A., Brechtel, F. J., and Wiedensohler, A.: A Tandem DMA for highly temperature-stabilized hygroscopic particle growth measurements between 90% and 98% relative humidity, *J. Aerosol Sci.*, 36, 1210-1223, doi:10.1016/j.jaerosci.2005.01.005, 2005.
- Horvath, H.: Estimation of the Average Visibility in Central Europe, *Atmos. Environ.*, 29, 241-246, doi:10.1016/1352-2310(94)00236-E, 1995.



- Hu, D., Qiao, L., Chen, J., Ye, X., Yang, X., Cheng, T., and Fang, W.: Hygroscopicity of inorganic aerosols: Size and Relative Humidity Effects on the Growth Factor, *Aerosol Air Qual. Res.*, 10, 255-264, doi:10.4209/aaqr.2009.12.0076, 2010.
- Johnson, G. R., Fletcher, C., Meyer, N., Modini, R., and Ristovski, Z. D.: A robust, portable H-TDMA for field use, *J. Aerosol Sci.*, 39, 850-861, doi:10.1016/j.jaerosci.2008.05.005, 2008.
- 5 Khalizov, A. F., Zhang, R., Zhang, D., Xue, H., Pagels, J. and McMurry, P. H.: Formation of highly hygroscopic soot aerosols upon internal mixing with sulfuric acid vapor, *J. Geophys. Res.*, 114, D05208, 1-15, doi:10.1029/2008JD010595, 2009.
- Kim, Y. J., Kim, K. W., Kim, S. D., Lee, B. K., and Han, J.S.: Fine particulate matter characteristics and its impact on visibility impairment at two urban sites in Korea: Seoul and Incheon, *Atmos. Environ.*, 40, S593–S605, doi: 10.1016/j.atmosenv.2005.11.076, 2006.
- 10 Lee, D. S., Fahey, D. W., Forster, P. M., Newton, P. J., Wit, R. C. N., Lim, L. L., Owen, B. and Sausen, R.: Aviation and global climate change in the 21st century, *Atmos. Environ.*, 43, 3520-3537, doi:10.1016/j.atmosenv.2009.04.024, 2009.
- Levy, J. I., Woody, M., Baek, B. H., Shankar, U., and Arunachalam, S.: Current and future particulate-matter-related mortality risks in the United States from aviation emissions during landing and takeoff, *Risk Analysis*, 32, 237-249, doi: 10.1111/j.1539-6924.2011.01660.x, 2012.
- 15 Lobo, P., Hagen, D. E., Whitefield, P. D., and Alofs, D. J.: Physical characterization of aerosol emissions from a commercial gas turbine engine, *J. Propul. Power*, 23, 919-929, doi:10.2514/1.26772, 2007.
- Lobo, P., Hagen, D. E., and Whitefield, P. D.: Measurement and analysis of aircraft engine PM emissions downwind of an active runway at the Oakland International Airport, *Atmos. Environ.*, 61, 114-123, doi:10.1016/j.atmosenv.2012.07.028, 2012.
- 20 Lobo, P., Hagen, D.E., and Whitefield, P.D.: Comparison of PM emissions from a Commercial Jet Engine burning Conventional, Biomass, and Fischer-Tropsch Fuels, *Environ. Sci. Technol.*, 45, 10744-10749, doi: 10.1021/es201902e, 2011.
- Lobo, P., Hagen, D. E., Whitefield, P. D., and Raper, D.: PM emissions measurements of in-service commercial aircraft engines during the Delta-Atlanta Hartsfield Study, *Atmos. Environ.*, 104, 237-245, doi:10.1016/j.atmosenv.2015.01.020,
- 25 2015a.
- Lobo, P., Christie, S., Khandelwal, B., Blakey, S.G, and Raper, D.W.: Evaluation of Non-volatile Particulate Matter Emission Characteristics of an Aircraft Auxiliary Power Unit with varying Alternative Jet Fuel Blend Ratios, *Energy Fuels*, 29, 7705-7711, doi: 10.1021/acs.energyfuels.5b01758, 2015b.
- Lobo, P., Condevaux, J., Yu, Z., Kuhlmann, J., Hagen, D.E., Miake-Lye, R.C., Whitefield, P.D., and Raper, D.W.:
30 Demonstration of a Regulatory Method for Aircraft Engine Nonvolatile PM Emissions Measurements with Conventional and Isoparaffinic Kerosene fuels, *Energy Fuels*, 30, 7770-7777, 10.1021/acs.energyfuels.6b01581, 2016.
- Lopez-Yglesias, X. F., Yeung, M. C., Dey, S. E., Brechtel, F. J., and Chan, C. K.: Performance evaluation of the Brechtel Mfg. Humidified Tandem Differential Mobility Analyzer (BMI HTDMA) for studying hygroscopic properties of aerosol particles, *Aerosol Sci. Technol.*, 48, 969-980, doi:10.1080/02786826.2014.952366, 2014.



- Massling, A., Leinert, S., Wiedensohler, A., and Covert, D.: Hygroscopic growth of sub-micrometer and one-micrometer aerosol particles measured during ACE-Asia, *Atmos. Chem. Phys.*, 7, 3249-3259, doi:10.5194/acp-7-3249-2007, 2007.
- Massling, A., Niedermeier, N., Hennig, T., Fors, E. O., Swietlicki, E., Ehn, M., Hameri, K., Villani, P., Laj, P., Good, N., McFiggans, G., and Wiedensohler, A.: Results and recommendations from an intercomparison of six Hygroscopicity-TDMA systems, *Atmos. Meas. Tech.*, 4, 485-497, doi:10.5194/amt 4 485 2011, 2011.
- McMurry, P. H. and Stolzenburg, M. R.: On the Sensitivity of Particle Size to Relative Humidity for Los Angeles Aerosols, *Atmos. Environ.*, 23, 497-507, doi:10.1016/0004-6981(89)90593-3, 1989.
- Meier, J., Wehner, B., Massling, A., Birmili, W., Nowak, A., Gnauk, T., Brüggemann, E., Herrmann, H., Min, H., and Wiedensohler, A.: Hygroscopic growth of urban aerosol particles in Beijing (China) during wintertime: a comparison of three experimental methods, *Atmos. Chem. Phys.*, 9, 6865-6880, doi:10.5194/acpd-9-6889-2009, 2009.
- Miake-Lye, R. C., Anderson, B. E., Cofer, W. R., Wallio, H. A., Nowicki, G. D., Ballenthin, J. O., Hunton, D. E., Knighton, W. B., Miller, T. M., Seeley, J. V., Viggiano, A. A.: SO_x oxidation and volatile aerosol in aircraft exhaust plumes depend on fuel sulfur content, *Geophys. Res. Lett.*, 25, 1677-1680, doi: 10.1029/98GL00064, 1998.
- Mikhailov, E., Vlasenko, S., Niessner, R., and Pöschl, U.: Interaction of aerosol particles composed of protein and salts with water vapor: hygroscopic growth and microstructural rearrangement, *Atmos. Chem. Phys.*, 34, 323-350, doi:10.5194/acp-4-323-2004, 2004.
- Moore, R. H., Shook, M., Beyersdorf, A., Corr, C., Herndon, S., Knighton, W. B., Miake-Lye, R., Thornhill, K. L., Winstead, E. L., Yu, Z., Ziemba, L. D., and Anderson, B. E.: Influence of Jet Fuel Composition on Aircraft Engine Emissions: A Synthesis of Aerosol Emissions Data from the NASA APEX, AAFEX, and ACCESS Missions, *Energy Fuels*, 29, 2591-2600, doi:10.1021/ef502618w, 2015.
- Onasch, T. B., Jayne, J. T., Herndon, S., Worsnop, D. R., Miake-Lye, R. C., Mortimer, I. P., and Anderson, B. E.: Chemical properties of aircraft engine particulate exhaust emissions, *J. Propul. Power*, 25, 1121-1137, doi:10.2514/1.36371, 2009.
- Park, K., Kim, J. S., and Miller, A. L.: A study on effects of size and structure on hygroscopicity of nanoparticles using a tandem differential mobility analyzer and TEM, *J. Nanopart. Res.*, 11, 175-183, doi:10.1007/s11051-008-9462-4, 2009a.
- Park, K., Kim, J. S., and Park, S. H.: Measurements of hygroscopicity and volatility of atmospheric ultrafine particles during ultrafine particle formation events at urban, industrial, and coastal sites, *Environ. Sci. Technol.*, 43, 6710-6716, doi:10.1021/es900398q, 2009b.
- Popovicheva, O., Persiantseva, N. M., Shonija, N. K., DeMott, P., Koehler, K., Petters, M., Kreidenweis, S., Tishkova, V., Demirdjian, B., and Suzanne, J.: Water interaction with hydrophobic and hydrophilic soot particles, *Phys. Chem. Chem. Phys.*, 10, 2332-2344, doi: 10.1039/b718944n, 2008.
- Pruppacher, H. R. and Klett, J. D.: *Microphysics of Clouds and Precipitation*, 1st Ed., D. Reidel Publishing Co, Dordrecht, Holland, 141-146, 1978.
- Reavell, K., Hands, T., and Collings, N.: A fast response particulate spectrometer for combustion aerosols. SAE Technical Paper, 2002-01-2714, doi: 10.4271/2002-01-2714, 2002.



- Robinson, R. A., and Stokes, R. H.: Electrolyte Solutions, 2nd Ed., Dover Publications, Mineola, New York, 2002.
- Rye, L., Lobo, P., Williams, P. I., Uryga-Bugajska, I., Christie, S., Wilson, C., Hagen, D., Whitefield, P., Blakey, S., Coe, H., Raper, D., Pourkashanian, M.: Inadequacy of Optical Smoke Measurements for Characterization of Non-Light Absorbing Particulate Matter Emissions from Gas Turbine Engines, *Combust. Sci. Technol.*, 184, 2068-2083, doi: 10.1080/00102202.2012.697499, 2012.
- Schmid, O.: Tandem differential mobility analyzer studies and aerosol volatility, Ph.D. thesis, University of Missouri-Rolla, Rolla, Missouri, USA, 65409, 2000. Saleh, R., Shihadeh, A., and Khlystov, A.: On transport phenomena and equilibration time scales in thermodenuders, *Atmos. Meas. Tech.*, 4, 571-581, doi:10.5194/amt-4-571-2011, 2011.
- Schumann, U., Arnold, F., Busen, R., Curtius, J., Kärcher, B., Kiendler, A., Petzold, A., Schlager, H., Schröder, F. and Wohlfrom, K. H.: Influence of fuel sulfur on the composition of aircraft exhaust plumes: The experiments SULFUR 1–7, *J. Geophys. Res.*, 107(D15), doi: 10.1029/2001JD000813, 2002.
- Shi, Y., Ge, M., and Wang, W.: Hygroscopicity of internally mixed aerosol particles containing benzoic acid and inorganic salts, *Atmos. Environ.*, 60, 9-17, doi.org/10.1016/j.atmosenv.2012.06.034, 2012.
- Staples, B. R.: Activity and osmotic coefficients of aqueous sulfuric acid at 298.15 K, *J. Phys. Chem. Ref. Data*, 10, 779-798, doi: 10.1063/1.555648, 1981.
- Suda, S. R., and Petters, M.: Accurate determination of aerosol activity coefficients at relative humidities up to 99% using the hygroscopicity tandem differential mobility analyzer technique, *Aerosol Sci. Technol.*, 47, 991-1000, doi:10.1080/02786826.2013.807906, 2013.
- Swietlicki, E., Hansson, H. C., Hämeri, K., Svenningsson, B., Massling, A., McFiggans, G., McMurry, P. H., Petäjä, T., Tunved, P., Gysel, M., Topping, D., Weingartner, E., Baltensperger, U., Rissler, J., Wiedensohler, A., and Kulmala, M.: Hygroscopic properties of submicrometer atmospheric aerosol particles measured with H-TDMA instruments in various environments—a review, *Tellus, Series B: Chemical and Physical Meteorology*, 60B, 432–469, doi:10.1111/j.1600-0889.2008.00350.x, 2008.
- Tang, I.N. Wong, W.T., and Munkelwitz, H.R.: The relative importance of atmospheric sulfates and nitrates in visibility reduction, *Atmos. Environ.*, 15, 2463-2471, doi:10.1016/0004-6981(81)90062-7, 1981.
- Timko, M.T., Yu, Z., Onasch, T.B., Wong, H.-W., Miake-Lye, R.C., Beyersdorf, A.J., Anderson, B.E., Thornhill, K L., Winstead, E.L., Corporan, E., DeWitt, M.J., Klingshirn, C.D., Wey, C., Tacina, K., Liscinsky, D.S., Howard, R., and Bhargava, A.: Particulate Emissions of Gas Turbine Engine Combustion of a Fischer-Tropsch Synthetic Fuel, *Energy Fuels*, 24, 5883-5896, doi: 10.1021/ef100727t, 2010.
- Timko, M. T., Fortner, E., Franklin, J., Yu, Z., Wong, H. W., Onasch, T. B., Miake-Lye, R. C., and Herndon, S. C.: Atmospheric measurements of the physical evolution of aircraft exhaust plumes, *Environ. Sci. Technol.*, 47, 3513-3520, doi:10.1021/es304349c, 2013.



- Unal, A., Hu, Y., Chang, M. E., Odman, M. T., and Russell, A. G.: Airport related emissions and impacts on air quality: Application to the Atlanta International Airport, *Atmos. Environ.*, 39, 5787-5798, doi: 10.1016/j.atmosenv.2005.05.051, 2005.
- Virkkula, A., Van Dingenen, R., Raes, F., and Hjorth, J.: Hygroscopic properties of aerosol formed by oxidation of limonene, α -pinene, and β -pinene, *J. Geophys. Res.*, 104, 3569-3579, doi:10.1029/1998JD100017, 1999.
- 5 Weingartner, E., Burtscher, H., and Baltensperger, U.: Hygroscopic properties of carbon and diesel soot particles, *Atmos. Environ.*, 31, 2311-2327, doi:10.1016/S1352-2310(97)00023-X, 1997
- Weingartner, E., Gysel, M., and Baltensperger, U.: Hygroscopicity of aerosol particles at low temperatures. 1. New low-temperature H-TDMA instrument: Setup and first applications, *Environ. Sci. Technol.*, 36, 55-62, doi:10.1021/es010054o, 10 2002.
- Wyslouzil, B. E., Carleton, K. L., Sonnenfroh, D. M., Rawlins, W. T., and Arnold, S.: Observation of hydration of single, modified carbon aerosols, *Geophys. Res. Lett.*, 21, 2107-2110, doi: 10.1029/94GL01588, 1994. Woods, E., Heylman, K. D., Gibson, A. K., Ashwell, A. P., and Rossi, S. R.: Effects of NO_y aging on the dehydration dynamics of model sea spray aerosols, *J. Phys. Chem. A*, 117, 4214-4222, doi:10.1021/jp401646d, 2013.
- 15 Woody, M., Baek, B. H., Adelman, Z., Omary, M., Lam, Y. F., West, J. J., and Arunachalam, S.: An assessment of aviation's contribution to current and future fine particulate matter in the United States, *Atmos. Environ.*, 45, 3424-3433, doi:10.1016/j.atmosenv.2011.03.041, 2011.
- Wu, Z., Birmili, W., Poulain, L., Wang, Z., Merkel, M., Fahlbusch, B., van Pinxteren, D., Herrmann, H., and Wiedensohler, A.: Particle hygroscopicity during atmospheric new particle formation events: implications for the chemical species 20 contributing to particle growth, *Atmos. Chem. Phys.*, 13, 6637-6646, doi:10.5194/acp-13-6637-2013, 2013
- Zhang, R., Khalizov, A. F., Pagels, J., Zhang, D., Xue, H., and McMurry, P. H.: Variability in morphology, hygroscopicity, and optical properties of soot aerosols during atmospheric processing, *Proc. Natl. Acad. Sci. USA*, 105, 10291-10296, doi:10.1073/pnas.0804860105, 2008.